Scripta Materialia 183 (2020) 50–54

Contents lists available at ScienceDirect

Scripta Materialia

journal homepage: www.elsevier.com/locate/scriptamat

Functional phase bistability in a nanocrystalline $RbMn[Fe(CN)_6]$ thin film fabricated by matrix-assisted laser evaporation

Dominik Maskowicz[a], Mirosław Sawczak[a], Rafał Jendrzejewski[a], Maria Gazda[b], Hiroko Tokoro[c], Shin-ichi Ohkoshi[d], Yann Garcia[e], Gerard Śliwiński[a,*]

[a] Department of Photophysics, Institute of Fluid Flow Machinery, Polish Academy of Sciences, Fiszera 14, 80-231 Gdańsk, Poland
[b] Department of Solid State Physics, Faculty of Applied Physics and Mathematics, Gdansk University of Technology, Narutowicza 11/12, 80-233 Gdańsk, Poland
[c] Division of Materials Science, Faculty of Pure and Applied Sciences, University of Tsukuba, Tenodai 1-1-1, Tsukuba, Ibaraki 305-8571, Japan
[d] Department of Chemistry, School of Science, University of Tokyo, 7-3-1 Hongo, Bunkyo-ku, Tokyo 113-0033, Japan
[e] Institute of Condensed Matter and Nanosciences, Molecular Chemistry, Materials and Catalysis division (IMCN/MOST), Université Catholique de Louvain, Place L. Pasteur 1, 1348 Louvain-La-Neuve, Belgium

ARTICLE INFO

Article history:
Received 14 February 2020
Revised 5 March 2020
Accepted 9 March 2020

Keywords:
Bistable-phase transition
Laser deposition
Thin films
Nanocrystalline materials
Raman spectroscopy

ABSTRACT

One of the main barriers hindering applications of Prussian blue metal assemblies is their poor processability, which makes the fabrication of intact thin films very difficult. In this work, a nanocrystalline $RbMn[Fe(CN)_6]\cdot xH_2O$ film on silicon substrate was obtained for the first time via laser-stimulated deposition and investigated. Temperature-induced phase transition and bistability within broad hysteresis loop (120 K), along with transition temperatures up to 317 K, which is the highest in the RbMnFe series, were observed using variable-temperature Raman spectroscopy. This study thus proposes a reliable deposition approach for preparing a functional magnetic materials that operate at room temperature.

Among the many functional coordination polymers (CPs), Prussian blue analogs are known for their unique properties and diverse fields of application, with particular importance in combatting global challenges in environmental and health research [1]. Indeed, Prussian blue analogs have attracted widespread attention owing to their promise for application in energy storage, sensing, capture and separation of volatile species, hydrogen storage, memory blocks [2–8], and photomagnetism [9]. This is closely related to the discovery of their unusual phase transition phenomena, which can change the optical, electric, and magnetic properties of the materials in response to a variety of stimuli such as heat, light, pressure, electric field, and chemical exposure [10–13]. The reported charge transfer-induced phase transition is exceptionally useful for switching property, because it changes electronic states of metal ions. Prussian blue analogs have the following structure: $AM[Fe(CN)_6]\cdot xH_2O$ (A = Li, Na, K, Rb, Cs; M = transition metal). In the cyano-bridged bimetal assembly $RbMn[Fe(CN)_6]\cdot xH_2O$, the transition between the so-called high-temperature (HT) and low-temperature (LT) phases corresponds to intermetallic electron transfer from Mn^{II} to Fe^{III} associated to a Jahn–Teller distortion of the produced Mn^{III} ion. The mechanism involves a thermally induced charge transfer between Mn^{II}–NC–Fe^{III} and Mn^{III}–NC–Fe^{II} pairs through cyano bridges. In addition, a structural HT to LT phase transition occurs between cubic ($F4^3$ m) and tetragonal ($I\bar{4}m2$) systems [14].

Such a phase change is associated with an exceptionally broad thermal hysteresis loop and light-induced reversible phase switching in the room-temperature region [15]. Both thermally and photoinduced phase changes are ascribed to the propagation of strong cooperative effects, which originate from the interaction of the crystal lattice strain with metal ions [16], as observed in spin crossover (SCO) CPs [17]. The effects of cooperativity on functional features have been reported for bulk, single crystal, microcrystalline, and nanoparticle (NP) materials, where for the latter the crystal downsizing effect decreases the extent of the bistable domain, with reentrance phenomena observed in the case of ultrasmall NPs [18–21].

Insertion of $RbMn[Fe(CN)_6]\cdot xH_2O$ into spintronic devices requires the production of intact thin films. However, developing a suitable reproducible thin film fabrication method that ensures the presence of the functional properties in the resulting ma-

* Corresponding author.
E-mail address: gerards@imp.gda.pl (G. Śliwiński).

https://doi.org/10.1016/j.scriptamat.2020.03.019
1359-6462/

terial is challenging [22,23]. This difficulty is attributed to the fragility of the porous network of CPs, which suffer under thermal stress and vacuum conditions, and to their poor processability, which is mainly related to the presence of $(CN)_6$ groups and lattice water molecules. As a consequence, requirements such as reproducible fabrication, control over the material properties, absence of by-products, and scalability are hard to meet, despite impressive advances and the wide variety of existing approaches available [24,25]. The properties of metal assembly thin films are particularly sensitive to imperfections associated with the deposition methods. For example, this was recently observed for PEG-impregnated {Fe(pyrazine)[Pt(CN)$_4$]} films produced by matrix-assisted pulsed-laser evaporation (MAPLE). These SCO thin films presented an unprecedented 100 K downshift of the hysteresis loop from room temperature [26]. Recently, vacuum sublimation has been suggested as the most reliable pathway for depositing SCO thin films, although the number of sublimable complexes remains rather limited [27–29]. This indicates that for switchable materials (such as RbMn[Fe(CN)$_6$]·xH$_2$O) that are non-evaporable, i.e. degrade irreversibly upon thermal and/or vacuum processing, an approach ensuring controlled fabrication of thin films is of the utmost importance, given their potentiality for use in spintronic devices.

This paper reports the first observation of bistable behavior in a thin film obtained by laser-induced deposition of the nanocrystalline Prussian blue analog RbMn[Fe(CN)$_6$]·xH$_2$O. Film samples obtained via a specially developed extension of the MAPLE method exhibit structural bistability owing to thermally stimulated, charge-transfer-induced phase transition within a broad thermal hysteresis loop around room temperature. The phase transition and structural properties of the produced thin film are described and discussed in detail.

The applied deposition process is based on laser ablation of a cryogenically frozen target, consisting of the material to be deposited suspended/dissolved in the matrix. During laser irradiation, the matrix material absorbs the applied laser pulses and protects the particles of the fragile compound Prussian blue from laser damage. Compared to the original MAPLE process designed for the deposition of organic, molecular, and other fragile materials [25], the extended method developed and applied in this study ensures additional process flexibility, which is mainly attributed to the controlled temperatures of the target and substrate. During the process, a stream of the compound particles moves towards the substrate and immobilizes on its surface, while the evaporated matrix is pumped away. The conditions and geometry of the laser interaction and the matrix material are carefully selected to ensure maximal absorption of the latter. The laser pulse energy is kept only slightly above the matrix ablation threshold in order to prevent compound decomposition and ablation of larger target fragments, which could negatively affect the structural uniformity of the deposition. The deposition is selective regarding the size distribution and size-to-weight ratio of the particles. Some of the particles are eliminated from the deposition process because they have either insufficient or excessive kinetic energy compared to that required for immobilization on the substrate.

The RbMn[Fe(CN)$_6$]·1·5H$_2$O (chemical composition $Rb^{I}Mn^{II}[Fe^{III}(CN)_6]_{0.96}[Fe^{II}(CN)_6]_{0.03}\cdot 1\cdot 5H_2O$) nanocrystalline powder was synthesized according to a procedure described elsewhere [19] and used in the form of a stable methanol suspension at a concentration of 6.2 ± 0.5 wt%. For preparation of the cryo-target, the suspension was diluted at a ratio of 1:5 with acetonitrile ensuring faster solidification and better matrix stability compared to methanol. The suspension was filled into a reservoir mounted on a cryostat COOLP 2/10 (Leybold) cooling block located in a vacuum chamber (backpressure = 10^{-6} mbar), and solidified at a temperature not exceeding 80 K.

For target ablation, we used a λ = 1064 nm laser Briliant B (Quantel) delivering 6 ns pulses at a 10 Hz repetition rate and the target was scanned by the laser beam focused using a lens (f = 400 cm) mounted on a motorized XY stage. A laser pulse energy of 50 mJ resulted in an energy density of 5.5 ± 0.5 J/cm^2 at the target surface. Monocrystalline 0.1 mm thick Si wafers (10 × 10 mm^2) sonicated in acetone, rinsed with isopropanol, and dried were used as the substrates. Prior to the deposition, the chamber was pressurized with N_2 at 1.05 bar and the film was deposited on a substrate preheated to 320 K at a target–substrate distance of 10 mm with a deposition rate of 10 ± 1.8 ng/min. Reference samples were prepared by drop-casting 25 µl of the RbMn[Fe(CN)$_6$] methanol dispersion on a glass substrate and drying under standard conditions.

Inspection of the uniform structure of the laser-deposited film observed in the scanning electron microscope images (SEM, FEI Quanta FEG 250) confirmed the presence of the original nanocrystalline material, which reveals the characteristic NP size distribution [19,30]. No damage to the NP surface or changes in shape were observed (Fig. 1(a)).

Interestingly, for the vast majority of NPs in the film, their largest surface is roughly parallel to that of the substrate, thus effectively increasing the surface coverage of the latter. This texturing is in agreement with the X-ray diffraction (XRD) pattern of the film obtained using an X-ray diffractometer X'Pert PRO MPD (PANalytical, Cu K_α line) and refined using the Rietveld method (Fig. 1(b)). The most intense reflections at (200) and (400) ascribed to the crystalline surfaces in-plane with the horizontally aligned NPs clearly dominate the pattern and, at the same time, suppress the intensity of the reflections from crystalline planes showing other inclinations [31].

Despite the relatively low XRD signal intensity of the thin film, the pattern agrees with that observed for plate-shaped crystals in the HT phase and is consistent with a face-centered cubic structure [14]. Most importantly, it indicates that the crystalline structure of the NPs is unaffected by laser-based deposition. Average thickness of the film estimated from the profilometer Dektak XT (Bruker, ball radius 2.5 µm) surface scan is X_{avg} = 72 nm (Fig. 1(c)). Peaks in the surface profile correspond to locally stacked NPs visible in the SEM image and suggest the deposition of aggregated particles. The discontinuities observed in the film are only partially related to the laser deposition, generally characterized by the Gaussian-like spatial distribution of species in the ablation plume and the random orientation of particles immobilized on the substrate [32]. While the careful selection of the process parameters can improve the film structure, it is the NP size and shape that ultimately determine the surface roughness and the lower limit of the film thickness.

The temperature-induced transition between the HT and LT phases was observed by Raman spectroscopy since the frequency of the CN stretching mode responds sensitively to the valence states of the neighboring Fe and Mn ions bridged by the cyano ligands [33]. Raman spectra were recorded at 320 K and 150 K for samples inserted in a liquid nitrogen-cooled cryostat module MicrostatN (Oxford Instruments) filled with an inert gas ($Ar_{(g)}$) and mounted on the XY positioning table of a micro-Raman spectrometer inVia (Renishaw). Samples were excited by a λ = 785 nm laser with the power reduced to 0.2 mW (see Appendix A – Supplementary material, Fig. S1).

The spectra of the laser-deposited film and the reference NPs acquired above room temperature (320 K) both show strong bands at 2164 and 2172 cm^{-1}, corresponding to the HT configuration of the Mn(II)–NC-Fe(III) complex (Fig. 2(a)) [18,33]. Upon cooling to 150 K, these bands were markedly decreased in both samples while new bands of a similar intensity appeared. The band at 2118 cm^{-1} is assigned to a cooperative charge-transfer-induced tran-

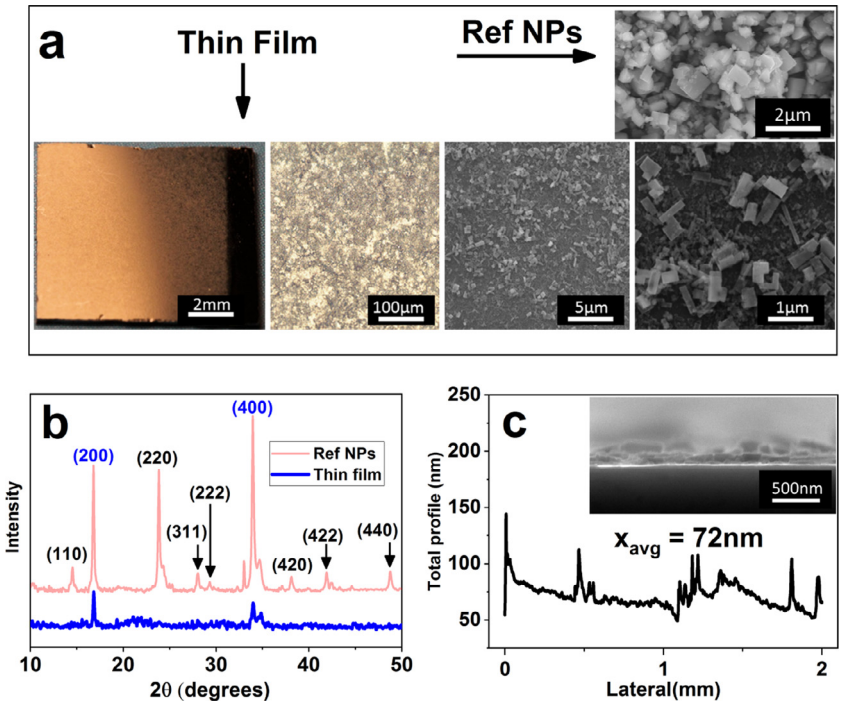

Fig 1. (a) SEM image of the reference NPs and optical microscope and SEM images of the thin film on the Si substrate (from left to right). (b) X-ray diffraction patterns of the reference NPs and the thin film on the SiO_2 substrates. (c) Peaks in the surface profile of the film on Si corresponding to stacked NPs/agglomerates revealed by SEM.

sition corresponding to the LT phase of Mn(III)–NC–Fe(II) while the band at 2098 cm^{-1} is assigned to the irregular Mn(II)–NC–Fe(II) configuration, which would require an equivalent Mn(III)–NC–Fe(III) configuration. Even though the corresponding band for the Mn(III)–NC–Fe(III) configuration is not observed, the coexistence of HT and LT phases (partial phase transition) and irregular configurations at the interface between the two phases cannot be excluded [18]. Differences in the spectra owing to changes in temperature are accompanied by a remarkable thermochromic effect (Fig. 2(b)), which is ascribed to a tautomeric conversion [17].

The exceptional capabilities of Raman spectroscopy were exploited further in the validation of the functional properties of the obtained film samples. This was performed via the temperature dependent discrimination of the HT and LT phases from Raman spectra (Appendix A, Fig. S2). In this work, it is of particular importance to determine whether the thin film exhibits HT–LT bistability and to measure the hysteretic behavior observed for the magnetic susceptibility of the reference NPs using a superconducting quantum interference magnetometer (SQUID MPMS, Quantum Design; Fig. 2(c)).

Indeed, in the case of the thin film, data extracted from spectra recorded at 10 K intervals and plotted as the intensity ratio of the characteristic bands at 2170 and 2114 cm^{-1} exhibit a hysteretic response characterized by phase transition temperatures of $T_{1/2}{}^{\downarrow} = 197$ K and $T_{1/2}{}^{\uparrow} = 317$ K, where $T_{1/2}{}^{\downarrow}$ and $T_{1/2}{}^{\uparrow}$ correspond to equally populated HT and LT phases upon cooling and heating, respectively (Fig. 2(d) and (e)). Compared to previous reports, the value of 317 K obtained for $T_{1/2}{}^{\uparrow}$ is the highest reported for RbMnFe assemblies to date [34]. The broadening of the hysteresis loop and the gradual spin population profile observed for the film could be related to a change in the NP size distribution due to laser interaction and/or laser-induced defects in the crystalline structure of the outermost layers of the NP surfaces. These local defects may hinder the heat propagation and thus affect the electron transfer. Modification of the water content should not be ruled out either. Indeed, laser heating can easily remove water molecules located in pores and defect sites in the $RbMn[Fe(CN)_6]$ crystal network, where adsorption of up to four H_2O molecules per primitive cell is possible [18]. While vacancies emerging from the absence of the Prussian blue ($Fe(CN)_6$) group can also reduce the stoichiometric concentration of Rb [35], the dominant effect of their replacement by structural water leads to stabilization of the HT state, resulting in a downshift of the HT–LT transition temperature upon cooling. It is also worth noting that the structural change corresponding to a water content greater than 2.5 molecules per primitive cell can lead to the complete loss of phase transition properties [36]. The 10 K difference in the $T_{1/2}{}^{\uparrow}$ determined by magnetic and Raman measurements for the NPs probably originates from the different experimental conditions (heat inertia, presence of residual water), while the difference between 304 K for the NPs and 317 K for the thin film is ascribed to the size-selective NP deposition. It is also a characteristic of the applied deposition process that the average NP size in the deposited film can be larger than that of the reference NPs, thus resulting in a positive shift of the hysteresis temperature and eventually its broadening. Thus, the nanostructuring of our material as a thin film produces an extension of the bistable domain, which increases both the spin stability range and thus the switchability in a broad operative range near room temperature which is a great advantage of $RbMn[Fe(CN)_6]$. The observed extent of the bistable domain also corresponds well to a previous report of NPs with size-dependent cooperative effects, which is advantageous from an application point of view [20].

In summary, this work provides the first evidence on a functional thin nanocrystalline film composed of a Prussian blue analog ($RbMn[Fe(CN)_6]\cdot 1\cdot 5H_2O$) obtained by laser-stimulated deposition. Film samples of up to 200 nm thickness consisting of cuboidal nanoparticles were fabricated on monocrystalline Si substrates by means of a specially developed extension of the MAPLE method. For deposition, the NP suspension at a concentration of around 1% in a methanol/acetonitrile mixture was solidified below 80 K and evaporated by pulsed-laser irradiation. Film samples deposited by the applied method exhibited crystallinity, which was confirmed by observation of the XRD patterns. The functionalities of the obtained film samples and their application potential were deter-

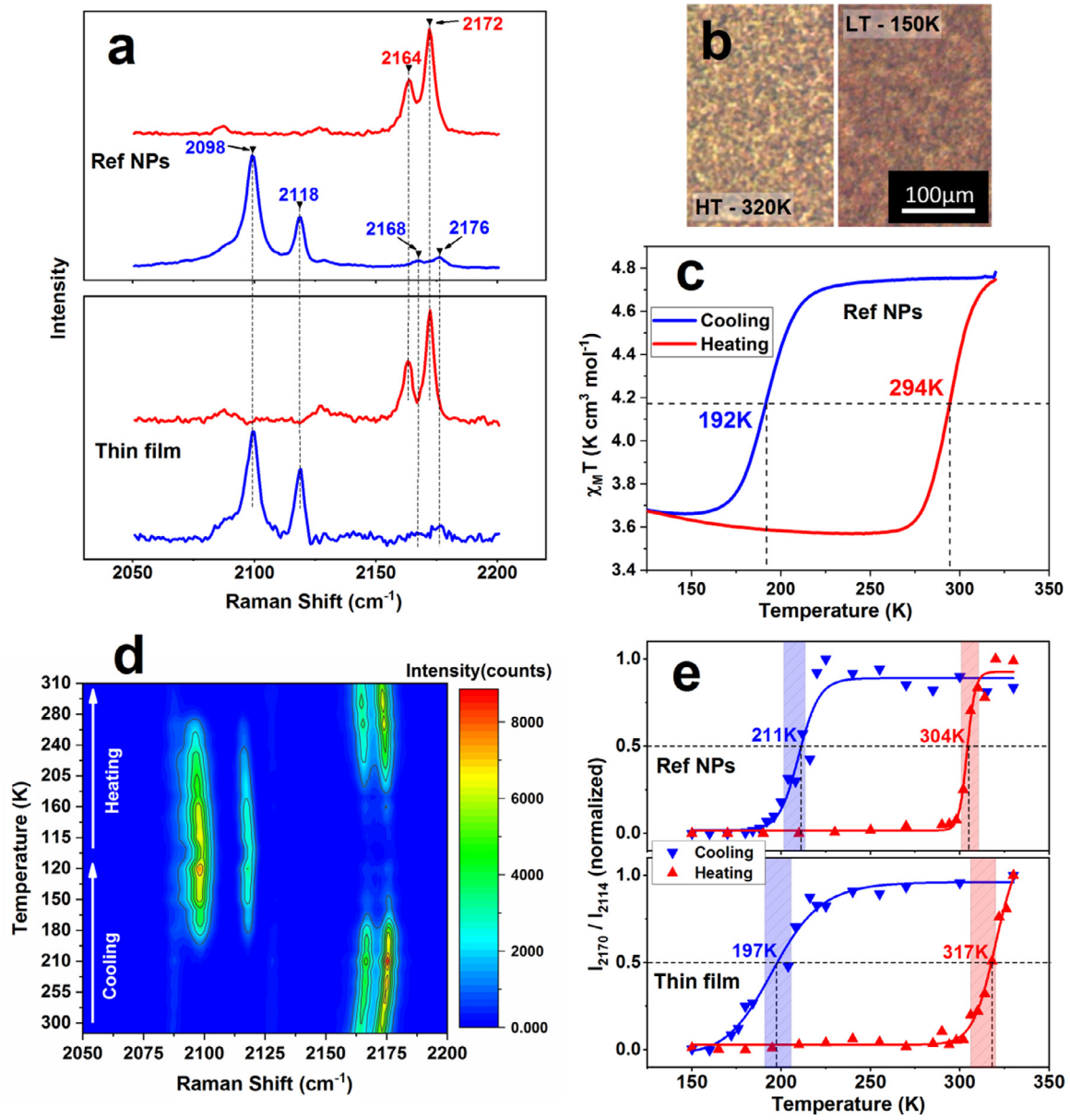

Fig 2. (a) Comparison of Raman spectra (excitation at $\lambda = 775$ nm) of the reference sample and the prepared thin film in both HT (323 K, red) and LT phases (150 K, blue). (b) Thin film: microscope observation revealed a color change from pale orange to deep red corresponding to the change in temperature from 320 K to 150 K. (c) Reference NPs: a broad hysteresis loop was observed in the temperature dependence of the magnetic susceptibility. (d) Thin film: intensity map of band intensities of the variable-temperature Raman spectra upon cooling and heating. (e) Temperature dependence of the intensity ratio of Raman bands at 2170 and 2114 cm^{-1} measured for the reference NPs and the prepared thin film. Data points are averages from 10 measurements and the blue and red regions indicate the temperature range where values were obtained for $T_{1/2}{}^{\downarrow}$ and $T_{1/2}{}^{\uparrow}$, respectively.

mined from phase transitions observed using variable-temperature Raman spectra. A wide thermal hysteresis loop (of width 120 K) and high LT → HT transition temperature up to $T_{1/2}{}^{\uparrow} = 317$ K was observed and ascribed to stabilization of the LT phase resulting from deposition-specific structural changes to the metal assembly. The coincidence of the phase transition with the accompanying thermochromic effect confirmed the functionality of the film. In particular, this means that the phase transition could also be induced by other stimuli, such as light, pressure, or adsorption of small molecules, analogous with previous reports. The postulated relation between the deposition-specific upshift of the NP size distribution and the broadening of the hysteresis loop indicates the stabilization of the LT phase and/or improved cooperativity of magnetic interactions in the thin film in comparison to the reference material, an effect worthy of further investigation. The results reported here refer to a representative compound for a broader family of spintronic materials, so this work provides a reliable route for the fabrication of thin films of these materials, thus opening a promising approach towards the development of functional spintronic devices.

Declaration of Competing Interest

None.

Acknowledgment

This work was supported by the joint research projects FNRS-PAN/CDR 33694457 and WBI-MNiSW/CDR 33694457. DM acknowledges support from project 2018/31/N/ST8/01797-NCN/Poland, and HT and S-IO via grants 15H05697 and KAKENHI 16H06521 of JSPS. Special thanks go to Dr. J. Karczewski for

providing access to SEM facility of Nanotech/GUT and to colleagues from COST Actions CA15128 and CA17123 for pertinent discussions.

Supplementary materials

Supplementary material associated with this article can be found, in the online version, at doi:10.1016/j.scriptamat.2020.03.019.

References

[1] Y. Guari, J. Larionova, Prussian Blue-Type Nanoparticles and Nanocomposites: Synthesis, Devices, and Applications, 1st ed., Jenny Stanford Publishing, New York, 2019.
[2] H. Tokoro, S. Ohkoshi, Dalton. Trans. 40 (2011) 6825–6833.
[3] M. Fitta, P. Czaja, M. Krupiński, G. Lewińska, M. Szuwarzyński, M. Bałanda, Chem. Select. 2 (2017) 7930–7934.
[4] M. Ishizaki, K. Kanaizuka, M. Abe, Y. Hoshi, M. Sakamoto, T. Kawamoto, H. Tanaka, M. Kurihara, Green Chem 14 (2012) 1537–1544.
[5] P.K. Thallapally, R.K. Motkuri, C.A. Fernandez, B.P. McGrail, G.S. Behrooz, Inorg. Chem. 49 (2010) 4909–4915.
[6] S.S. Kaye, J.R. Long, J. Am. Chem. Soc. 127 (2005) 6506–6507.
[7] M. Yang, J. Jiang, Y. Yang, X. Chen, G. Shen, R. Yu, Biosens. Bioelectron. 21 (2006) 1791–1797.
[8] T. Shibata, Y. Fukuzumi, Y. Moritomo, Sci. Rep. 8 (2018) 14784.
[9] P. Gütlich, Y. Garcia, Th. Woike, Coord. Chem. Rev. 219–221 (2001) 839–879.
[10] H. Tokoro, S. Ohkoshi, Bull. Chem. Soc. Jpn. 88 (2015) 227–239.
[11] X. Liu, Y. Moritomo, T. Matsuda, H. Kamioka, H. Tokoro, S. Ohkoshi, J. Phys. Soc. Jpn. 78 (2009) 013602.
[12] L. Egan, K. Kamenev, D. Papanikolaou, Y. Takabayashi, S. Margadonna, J. Am. Chem. Soc. 128 (2006) 6034–6035.
[13] H. Tokoro, T. Matsuda, T. Nuida, Y. Moritomo, K. Ohoyama, E.D.L. Dangui, K. Boukheddaden, S. Ohkoshi, Chem. Mater. 20 (2008) 423–428.
[14] H. Tokoro, S. Ohkoshi, T. Matsuda, K. Hashimoto, Inorg. Chem. 43 (2004) 5231–5236.
[15] H. Tokoro, S. Ohkoshi, Springer, Berlin, Heidelberg, 2013, pp. 693–727.
[16] V. Niel, J.M. Martinez-Agudo, M.C. Muñoz, A.B. Gaspar, J.A. Real, Inorg. Chem. 40 (2001) 3838–3839.
[17] P. Gütlich, A.B. Gaspar, Y. Garcia, Beilstein J. Org. Chem. 9 (2013) 342–391.
[18] E.J.M. Vertelman, T.T.A. Lummen, A. Meetsma, M.W. Bouwkamp, G. Molnar, P.H.M. van Loosdrecht, P.J. van Koningsbruggen, Chem. Mater. 20 (2008) 1236–1238.
[19] H. Tokoro, K. Nakagawa, K. Imoto, F. Hakoe, S. Ohkoshi, Chem. Mater. 24 (2012) 1324–1330.
[20] G. Félix, W. Nicolazzi, L. Salmon, G. Molnár, M. Perrier, G. Maurin, J. Larionova, J. Long, Y. Guari, A. Bousseksou, Phys. Rev. Lett. 110 (2013) 235701.
[21] H. Peng, S. Tricard, G. Félix, G. Molnár, W. Nicolazzi, L. Salmon, A. Bousseksou, Angew. Chem. Int. Ed. 53 (2014) 10894–10898.
[22] M. Cavallini, Phys. Chem. Chem. Phys. 14 (2012) 11867–11876.
[23] M.B. Zakaria, T. Chikyow, Coord. Chem. Rev. 352 (2017) 328–345.
[24] K. Otsubo, T. Haraguchi, H. Kitagawa, Coord. Chem. Rev. 346 (2017) 123–138.
[25] A.D. Stiff-Roberts, W. Ge, Appl. Phys. Rev. 4 (2017) 41303.
[26] M. Sawczak, R. Jendrzejewski, D. Maskowicz, Y. Garcia, A.C. Ghosh, M. Gazda, J. Czechowski, G. Śliwiński, Eur. J. Inorg. Chem. 2019 (2019) 3249–3255.
[27] M. Ruben, K.S. Kumar, Angew. Chem. Int. Ed. (2019), doi:10.1002/anie.201911256.
[28] V. Shalabaeva, S. Rat, M.D. Manrique-Juarez, A.-C. Bas, L. Vendier, L. Salmon, G. Molnár, A. Bousseksou, J. Mater. Chem. C 5 (2017) 4419–4425.
[29] G. Molnár, S. Rat, L. Salmon, W. Nicolazzi, A. Bousseksou, Adv. Mater. 30 (2018) 1703862.
[30] P.K. Phu, N.M. Thuan, N.V. Minh, J. Exp. Nanosci. 7 (2012) 336–343.
[31] H.J. Bunge, Texture. Microstruct. 29 (1997) 1–26.
[32] T. Ikegami, S. Ishibashi, Y. Yamagata, K. Ebihara, R.K. Thareja, J. Narayan, J. Vac. Sci. Technol. A 19 (2001) 1304–1307.
[33] R. Fukaya, M. Nakajima, H. Tokoro, S. Ohkoshi, T. Suemoto, J. Chem. Phys. 131 (2009) 154505.
[34] H. Tokoro, T. Matsuda, K. Hashimoto, S. Ohkoshi, J. Appl. Phys. 97 (2005) 10M508.
[35] S. Cobo, R. Fernández, L. Salmon, G. Molnár, A. Bousseksou, Eur. J. Inorg. Chem. 2007 (2007) 1549–1555.
[36] E.J.M. Vertelman, E. Maccallini, D. Gournis, P. Rudolf, T. Bakas, J. Luzon, R. Broer, A. Pugzlys, T.T.A. Lummen, P.H.M. van Loosdrecht, P.J. van Koningsbruggen, Chem. Mater. 18 (2006) 1951–1963.